Article

Alkene Hydrogenation on an 11-Vertex Rhodathiaborane with Full Cluster Participation

A#lvaro A#lvarez, Ramo#n Maci#as, Jonathan Bould, Mari#a Jose# Fabra, Fernando J. Lahoz, and Luis A. Oro

J. Am. Chem. Soc., **2008**, 130 (34), 11455-11466 • DOI: 10.1021/ja802993m • Publication Date (Web): 02 August 2008

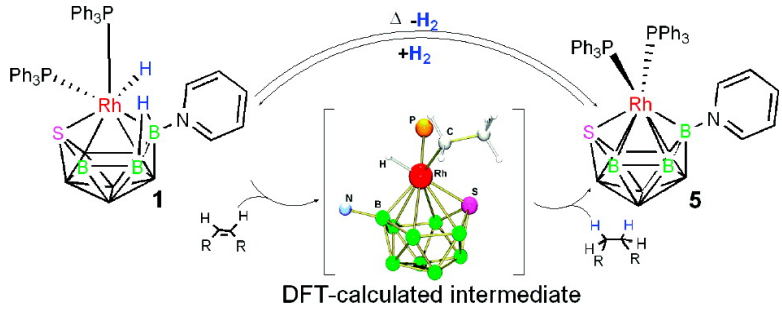

More About This Article

Additional resources and features associated with this article are available within the HTML version:

- Supporting Information
- Access to high resolution figures
- Links to articles and content related to this article
- Copyright permission to reproduce figures and/or text from this article

View the Full Text HTML

J|A|C|S
ARTICLES

Published on Web 08/02/2008

Alkene Hydrogenation on an 11-Vertex Rhodathiaborane with Full Cluster Participation

Álvaro Álvarez,[†] Ramón Macías,*[,†] Jonathan Bould,[§,⊥] María José Fabra,[‡] Fernando J. Lahoz,[‡] and Luis A. Oro[†,‡]

Departamento de Química Inorgánica, Instituto Universitario de Catálisis Homogénea, Instituto de Ciencia de Materiales de Aragón, Universidad de Zaragoza-Consejo Superior de Investigaciones Científicas, 50009-Zaragoza, Spain, Institute of Inorganic Chemistry, Academy of Sciences of the Czech Republic 250 68 Husinec-Řež 1001, Czech Republic, and School of Chemistry, University of Leeds, LS2 9JT, United Kingdom

Received April 23, 2008; E-mail: rmacias@unizar.es

Abstract: The facile synthesis of the metallaheteroborane [8,8-$(PPh_3)_2$-*nido*-8,7-$RhSB_9H_{10}$] (**1**) makes possible the systematic study of its reactivity. Addition of pyridine to **1** gives in high yield the 11-vertex *nido*-hydridorhodathiaborane [8,8,8-$(PPh_3)_2$H-9-(NC_5H_5)-*nido*-8,7-$RhSB_9H_9$] (**2**). **2** reacts with C_2H_4 or CO to form [1,1-(PPh_3)(L)-3-(NC_5H_5)-*closo*-$RhSB_9H_8$] [L = C_2H_4 (**3**), CO (**4**)]. In CH_2Cl_2 at reflux temperature **2** undergoes a *nido* to *closo* transformation to afford [1,1-$(PPh_3)_2$-3-(NC_5H_5)-*closo*-1,2-$RhSB_9H_8$] (**5**). Reaction of **2** with alkenes leads to hydrogenation and isomerization of the olefins. NMR spectroscopy indicates the presence of a labile phosphine ligand in **2**, and DFT calculations have been used to determine which of the two phosphine groups is labile. Rationalization of the hydrogenation mechanism and the part played by the **2** → **3** *nido* to *closo* cluster change during the reaction cycle is suggested. In the proposed mechanism the classical hydrogen transfer from hydride metal complexes to olefins occurs twice: first upon coordination of the alkene to the rhodium centre in **2**, and second concomitant with formation of a *closo*-hydridorhodathiaborane intermediate by migration of a BHB-bridging hydrogen atom to the metal. Reaction of H_2 with **3** or **5** regenerates **2**, closing a reaction cycle that under catalytic conditions is capable of hydrogenating alkenes. Single-site versus cluster-bifunctional mechanisms are discussed as possible routes for H_2 activation.

Introduction

The high-yield synthesis of the metallaheteroborane [8,8-$(PPh_3)_2$-*nido*-8,7-$RhSB_9H_{10}$] (**1**)[1] from [$RhCl(PPh_3)_3$] and Cs-[SB_9H_{12}] makes the systematic reaction chemistry of this compound accessible. For example, it has been observed that monodentate or bidentate phosphine ligands can replace the metal-bound PPh_3 groups in **1** and also fill the vacant coordination site on the formally 16-electron rhodium center. Alternatively, some phosphine ligands have been found to substitute the *exo*-terminal hydrogen atom on the boron vertex at the 9 position of **1**.[2–5] These reactions have resulted in the preparation of a series of 11-vertex *nido*-rhodathiaboranes of general formulae [8,8,8-$(L)_2(L')$-*nido*-8,7-$RhSB_9H_{10}$] (L, L′ = PMe_2Ph; L = PPh_3, L′ = CO; L = PPh_3, L′ = CH_3CN; L = η^2-dppm, L′ = η^1-dppm) and [8,8,8-H(η^2-L_2)-*nido*-8,7-$RhSB_9H_9$-9-(η^1-L_2)] (L_2 = dppe, dppp). Further observation made while studying these systems was a *nido* to *closo* transformation in the clusters with formal release of H_2 leading to 11-vertex *closo*-rhodathiaboranes with B−L bonds.[2,3] Some of these metallathiaboranes have interesting structures and chemistry. For example, [8,8,8-(η^2-dppm)(η^1-dppm)-*nido*-8,7-$RhSB_9H_{10}$] reacts with BH_3·THF to give an 11-vertex rhodathiaborane in which a BH_3 adduct coordinates to the rhodium atom in a bidentate fashion via its hydrogen atoms.[6] Recently, we extended this family of 11-vertex metallathiaboranes with the development of an effective route to N-heterocyclic-ligated clusters from reactions of [Rh(η^4-diene)(L_2)] [diene = cod or nbd; L_2 = bpy, Me_2bpy, phen, $(py)_2$] with $Cs[SB_9H_{12}]$.[7] This synthetic procedure allows the preparation of hybrid salts [Rh(η^4diene)(L_2)][SB_9H_{12}] that afford unsaturated and saturated clusters of general formulation [8,8-(L_2)-*nido*-$RhSB_9H_{10}$] [L_2 = bpy, Me_2bpy, phen, $(py)_2$] and [8,8,8-(L_2)(L′)-*nido*-$RhSB_9H_{10}$] (L_2 = bpy, Me_2bpy, phen; L′ = PPh_3 or CH_3CN), respectively. This group of 11-vertex rhodathiaboranes is an emerging example of the potential for

[†] Instituto Universitario de Catálisis Homogénea.
[‡] Instituto de Ciencia de Materiales de Aragón.
[§] Academy of Sciences of the Czech Republic.
[⊥] University of Leeds.

(1) Ferguson, G.; Jennings, M. C.; Lough, A. J.; Coughlan, S.; Spalding, T. R.; Kennedy, J. D.; Fontaine, X. L. R.; Stibr, B. *J. Chem. Soc., Chem. Commun.* **1990**, 891–894.
(2) Macías, R.; Rath, N. P.; Barton, L. *Organometallics* **1999**, *18*, 3637–3648.
(3) Coughlan, S.; Spalding, T. R.; Ferguson, G.; Gallagher, J. F.; Lough, A. J.; Fontaine, X. L. R.; Kennedy, J. D.; Stibr, B. *J. Chem. Soc., Dalton Trans.* **1992**, 2865–2871.
(4) Adams, K. J.; McGrath, T. D.; Rosair, G. M.; Weller, A. S.; Welch, A. J. *J. Organomet. Chem.* **1998**, *550*, 315–329.
(5) Ferguson, G.; Lough, A. L.; Coughlan, S.; Spalding, T. R. *Acta Crystallogr., Sect. C: Cryst. Struct. Commun.* **1992**, *C48*, 440–443.
(6) Macías, R.; Rath, N. P.; Barton, L. *Angew. Chem., Int. Ed.* **1999**, *38*, 162–164.
(7) Alvarez, A.; Macías, R.; Fabra, M. J.; Martin, M. L.; Lahoz, F. J.; Oro, L. A. *Inorg. Chem.* **2007**, *46*, 6811–6826.

novel chemistry that exists in metallaheteroboranes other than metallacarboranes.

The reactivity of metallaboranes and metallacarboranes with unsaturated organic molecules is well documented,[8–14] and the outcomes are interesting and diverse. In some cases, the metallaborane clusters react with the unsaturated molecule, leading to insertion of heteroatoms,[9,14] reduction of the organic substrate, or both.[10,12] Some of the reported reactions are remarkable. For example, reaction of the iridaborane [6,6-(PPh_3)H-μ-6^P,5^C-$(Ph_2P$-*o*-$C_6H_4)$-*nido*-6-IrB_9H_{12}] with acetylene affords [1,1,1-(C_4H_4)-μ-1^P,2^C-$(Ph_2P$-*o*-$C_6H_4)$-*isocloso*-1-IrB_9H_7-5-(PPh_3)] and [10-(PPh_3)-2,2,2-$(PH_3)_2(Ph_2P$-*o*-$C_6H_4)$-*closo*-2-IrB_9H_7-1].[15] The former compound is the result of dimerization of HCCH at the metal center, whereas the latter is the result of the reductive stripping of PPh_3 ligands and a *nido* to *closo* cluster transformation. Other reductions of alkynes by metallaboranes are better understood and lead to highly functionalized metallaboranes with organic substituents at the boron vertices.[12]

In polyhedral boron chemistry it has long been a goal to develop catalytic cycles by combining the oxidative and coordinative flexibility of transition-metal elements with the capability of boron clusters to exhibit oxidative/reductive flexibility in their classical *closo*−*nido*−*arachno* transformations. Some metallaboranes do exhibit catalytic activity in, for example, oligomerization of alkynes,[16] but although significant examples exist,[17–19] polyhedral boron chemistry shows a marked lack of reaction cycles either catalytic or stoichiometric. Of these, the catalytic hydrogenation and isomerization of olefins by 12-vertex rhodadicarboranes are probably the best-known catalytic processes in boron chemistry.[20–26] These pioneering studies led to new mechanisms that later served as inspiration for the development of new rhodacarboranes and metal complexes partnered with monocarborane ligands, which exhibit catalytic activity in the hydrogenation of olefins.[27–33] These studies, however, have not given rise to fundamental new mechanisms for either activation of H_2 or hydrogenation and isomerization of olefins. Here we report on the reactivity of 11-vertex *nido*- and *closo*-rhodathiaboranes with alkenes and H_2, which reveals new mechanisms for hydrogenation of olefins and activation of H_2 where the flexible structure of the metallaheteroborane cluster fully participates in the reactions.

Results and Discussion

Scheme 1 can be used as a guide to the sections that follow. The synthesis and selected reactivity of **2** and **3** have been described earlier.[34] Herein we discuss the structures and reactivities of these 11-vertex clusters in more detail and present the energy-optimized structures of these and some new rhodathiaboranes as well as gauge-independent atomic orbital (GIAO) NMR nuclear shielding predictions. Additionally, the behavior of **2** in its reaction with ethene is analyzed using DFT calculations, leading to new proposed mechanisms for the activation of dihydrogen and the catalytic isomerization and hydrogenation of olefins by these rhodathiaboranes.

[8,8,8-$(PPh_3)_2$H-9-(NC_5H_5)-*nido*-8,7-$RhSB_9H_9$] (2). Reaction of [8,8-$(PPh_3)_2$-*nido*-8,7-$RhSB_9H_{10}$] (**1**) with a 4-fold excess of pyridine at room temperature affords the *nido*-hydridorhodathiaborane **2** in 75 % yield. The solid-state structure of **2** comprises an 11-vertex *nido*-$RhSB_9$ skeleton of the same type as the parent compound **1** (Figure 1). Electronically, however, **2** has an additional skeletal electron pair (13 sep), conforming to the electron counting formalism,[35,36] and it is thus saturated with respect its precursor **1** (12 sep). This does not, however, lead to substantial differences of intramolecular distances and angles between **1** and **2** (Table 1). It is noteworthy, nevertheless, that **1** exhibits a larger disparity in the Rh−P distances than its pyridine-ligated derivative **2**. The longest Rh−P distance between the two compounds corresponds to the PPh_3 trans to the B(3)−B(4) edge in **1** (see Figure 1 for cluster numbering). Interestingly, the disposition of the two PPh_3 ligands with respect to the {$RhSB_9$} fragment changes upon reaction with the N-heterocyclic ligand, yielding a configuration with one PPh_3 group trans to the B(3)−B(4) edge and the other trans to the boron in the 9 position. The metal hydride occupies the third pseudo-octahedral metal position trans to the sulfur atom, which, in the unsaturated rhodathiaborane **1**, is occupied by a PPh_3

(8) Kalb, W. C.; Demidowicz, Z.; Speckman, D. M.; Knobler, C.; Teller, R. G.; Hawthorne, M. F. *Inorg. Chem.* **1982**, *21*, 4027–4036.
(9) de Montigny, F.; Macías, R.; Noll, B. C.; Fehlner, T. P.; Costuas, K.; Saillard, J.-Y.; Halet, J.-F. *J. Am. Chem. Soc.* **2007**, *129*, 3392–3401.
(10) Yan, H.; Noll, B. C.; Fehlner, T. P. *J. Organomet. Chem.* **2006**, *691*, 5060–5064.
(11) Fehlner, T. P. *Pure Appl. Chem.* **2006**, *78*, 1323–1331.
(12) Yan, H.; Noll, B. C.; Fehlner, T. P. *J. Am. Chem. Soc.* **2005**, *127*, 4831–4844.
(13) Bould, J.; Bown, M.; Coldicott, R. J.; Ditzel, E. J.; Greenwood, N. N.; Macpherson, I.; MacKinnon, P.; Thornton-Pett, M.; Kennedy, J. D. *J. Organomet. Chem.* **2005**, *690*, 2701–2720.
(14) Bould, J.; Rath, N. P.; Barton, L. *Organometallics* **1996**, *15*, 4916–4929.
(15) Bould, J.; Brint, P.; Fontaine, X. L. R.; Kennedy, J. D.; Thornton-Pett, M. *J. Chem. Soc., Chem. Commun.* **1989**, 1763–1765.
(16) Yan, H.; Beatty, A. M.; Fehlner, T. P. *Angew. Chem., Int. Ed.* **2001**, *40*, 4498–4501.
(17) Kadlecek, D. E.; Carroll, P. J.; Sneddon, L. G. *J. Am. Chem. Soc.* **2000**, *122*, 10868–10877.
(18) Littger, R.; Englich, U.; Ruhlandt-Senge, K.; Spencer, J. T. *Angew. Chem. Int. Ed* **2000**, *39*, 1472–1474.
(19) Macías, R.; Fehlner, T. P.; Beatty, A. M. *Angew. Chem. Int. Ed.* **2002**, *41*, 3860–3862.
(20) Long, J. A.; Marder, T. B.; Behnken, P. E.; Hawthorne, M. F. *J. Am. Chem. Soc.* **1984**, *106*, 2979–2989.
(21) Behnken, P. E.; Busby, D. C.; Delaney, M. S.; King, R. E.; Kreimendahl, C. W.; Marder, T. B.; Wilczynski, J. J.; Hawthorne, M. F. *J. Am. Chem. Soc.* **1984**, *106*, 7444–7450.
(22) Baker, R. T.; Delaney, M. S.; King, R. E.; Knobler, C. B.; Long, J. A.; Marder, T. B.; Paxson, T. E.; Teller, R. G.; Hawthorne, M. F. *J. Am. Chem. Soc.* **1984**, *106*, 2965–2978.
(23) Knobler, C. B.; Marder, T. B.; Mizusawa, E. A.; Teller, R. G.; Long, J. A.; Behnken, P. E.; Hawthorne, M. F. *J. Am. Chem. Soc.* **1984**, *106*, 2990–3004.
(24) Long, J. A.; Marder, T. B.; Hawthorne, M. F. *J. Am. Chem. Soc.* **1984**, *106*, 3004–3010.
(25) Behnken, P. E.; Belmont, J. A.; Busby, D. C.; Delaney, M. S.; King, R. E.; Kreimendahl, C. W.; Marder, T. B.; Wilczynski, J. J.; Hawthorne, M. F. *J. Am. Chem. Soc.* **1984**, *106*, 3011–3025.
(26) Belmont, J. A.; Soto, J.; King, R. E.; Donaldson, A. J.; Hewes, J. D.; Hawthorne, M. F. *J. Am. Chem. Soc.* **1989**, *111*, 7475–7486.
(27) Teixidor, F.; Nuñez, R.; Flores, M. A.; Demonceau, A.; Viñas, C. *J. Organomet. Chem.* **2000**, *614*−*615*, 48–56.
(28) Teixidor, F.; Flores, M. A.; Vinas, C.; Kivekas, R.; Sillanpaa, R. *Angew. Chem., Int. Ed.* **1996**, *35*, 2251–2253.
(29) Vinas, C.; Flores, M. A.; Nunez, R.; Teixidor, F.; Kivekas, R.; Sillanpaa, R. *Organometallics* **1998**, *17*, 2278–2289.
(30) Douglas, T. M.; Molinos, E.; Brayshaw, S. K.; Weller, A. S. *Organometallics* **2007**, *26*, 463–465.
(31) Moxham, G. L.; Douglas, T. M.; Brayshaw, S. K.; Kociok-Kohn, G.; Lowe, J. P.; Weller, A. S. *Dalton Trans.* **2006**, 5492–5505.
(32) Molinos, E.; Kociok-Kohn, G.; Weller, A. S. *Chem. Commun.* **2005**, 3609–3611.
(33) Rifat, A.; Patmore, N. J.; Mahon, M. F.; Weller, A. S. *Organometallics* **2002**, *21*, 2856–2865.
(34) Alvarez, A.; Macías, R.; Fabra, M. J.; Lahoz, F. J.; Oro, L. A. *J. Am. Chem. Soc.* **2008**, *130*, 2148–2149.
(35) Wade, K. *Adv. Inorg. Chem. Radiochem.* **1976**, *18*, 1–66.
(36) Mingos, D. M. P.; Wales, D. J. *Introduction to Cluster Chemistry*; Prentice Hall: London, 1990.

Scheme 1

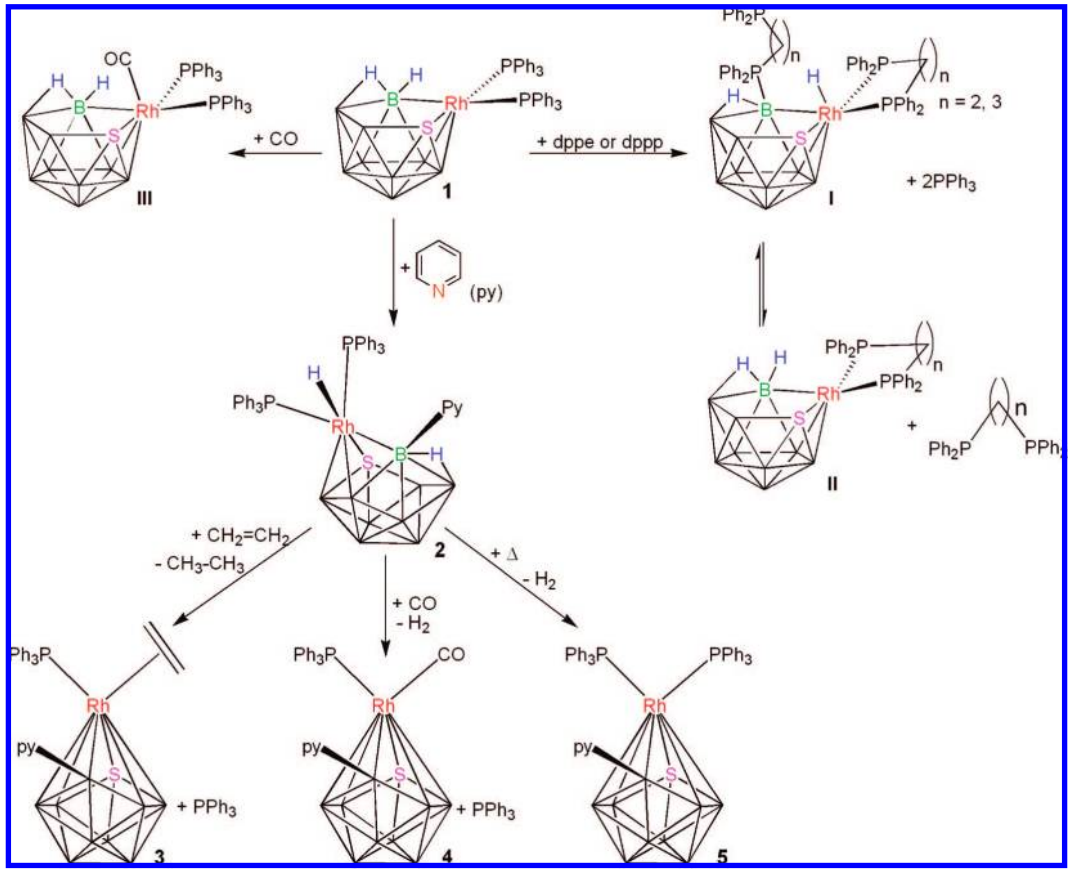

ligand. The length of the N−B distance falls within the reported range of 1.230−1.978 Å found for this type of interaction (CSD search, version 5.29).

Although the two Rh−P distances in **2** are similar, the variable-temperature $^{31}P\{^{1}H\}$ NMR spectra demonstrate that one PPh_3 ligand is labile, undergoing a fast dissociation at ambient temperature. In order to ascertain the position of the labile phosphine, we performed a relaxed scan of the potential-energy surface on the model [8,8,8-$(PH_3)_2$H-9-(NC_5H_5)-*nido*-8,7-$RhSB_9H_9$] (**2a**) by varying the Rh−P distances of the phosphines. The results of these studies are summarized in Figure 2, which illustrates that elongation of the PPh_3 trans to the B(3)−B(4) edge [P(2) in Figure 2] leads to a higher destabilization of the cluster, and we therefore conclude that the PPh_3 ligand trans to the pyridine-ligated boron atom B(9) is the labile phosphine [P(1) in Figure 2]. Elongation of P(1) in the model compound **2a** from the energy-optimized Rh−P distance of 2.4−4.0 Å leads to an increase in energy of 56 kJ/mol. This energy difference is very similar to the experimentally determined $\Delta G^{\ddagger}_{278}$ of 55 kJ/mol.

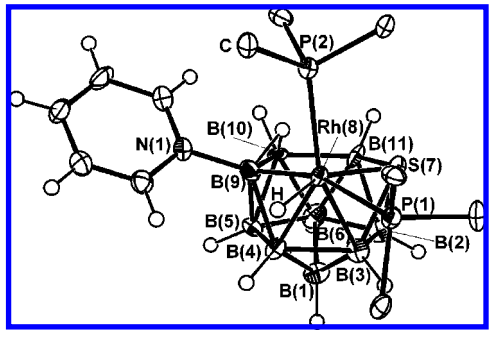

Figure 1. Molecular structure of [8,8,8-$(PPh_3)_2$H-9-(NC_5H_5)-*nido*-8,7-$RhSB_9H_9$] (**2**).

Table 2 gathers the measured NMR data of [8,8-$(PPh_3)_2$-*nido*-8,7-$RhSB_9H_{10}$] (**1**) together with those for [8,8,8-$(PPh_3)_2$H-9-(NC_5H_5)-*nido*-8,7-$RhSB_9H_9$] (**2**). A comparison of GIAO NMR shift calculations with ^{11}B NMR measured data was used to assign individual boron resonances to structural positions as defined by X-ray crystallography. The calculated values in Table 2 are presented in brackets. The agreement between the computed ^{11}B chemical shifts for [8,8-$(PH_3)_2$-*nido*-8,7-$RhSB_9H_{10}$] (**1a**) and [8,8,8-$(PH_3)_2$H-9-(NC_5H_5)-*nido*-8,7-$RhSB_9H_9$] (**2a**) and the measured values for compounds **1** and **2** are satisfactory, indicating that the DFT-calculated structures are good models of the crystallographically determined structures. It is interesting to note that the ^{1}H NMR resonance of the BHB bridging hydrogen atom in the hydridorhodathiaborane exhibits a shift to high field of 0.07 ppm with respect to that of **1**, a small change considering that the BHB resonance is very sensitive to substitution at either the rhodium center or the boron atom at the 9 position.[7] Overall, the ^{11}B NMR spectrum of **2** exhibits a slight shielding with respect to that of **1**. It is surprising however that the ^{11}B chemical shift of the pyridine-substituted boron atom located at the 9 position in **2** does not significantly change with respect to the parent unsubstituted rhodathiaborane **1**. These observations suggest that the higher electron density in **2** is delocalized over the whole framework, and we therefore attribute the labile nature of one of the PPh_3 ligands to the global effect of the N-substituted {$RhSB_9$} cluster rather than to localized trans effects.

Table 1. Selected Interatomic Distances (Å) for **2** and **3** with Estimated Standard Uncertainties (s.u.) in Parentheses[a]

2		**3**	
Rh(8)−S(7)	2.431(2)[2.431]	Rh(1)−S(2)	2.3721(8) [2.453]
Rh(8)−P(1)	2.354(2)[2.387]	Rh(1)−P(1)	2.2980(8) [2.311]
Rh(8)−P(2)	2.341(2)[2.347]	Rh(1)−C(1)	2.171(4) [2.205]
Rh(8)−B(3)	2.201(10)[2.303]	Rh(1)−C(2)	2.166(4) [2.200]
Rh(8)−B(4)	2.217(11)[2.243]	Rh(1)−B(3)	2.080(4) [2.094]
Rh(8)−B(9)	2.220(9)[2.201]	Rh(1)−B(4)	2.503(4) [2.516]
S(7)−B(2)	1.980(9)[1.999]	Rh(1)−B(5)	2.427(4) [2.590]
S(7)−B(3)	2.059(11)[2.073]	Rh(1)−B(6)	2.365(4) [2.396]
S(7)−B(11)	1.953(9)[1.943]	Rh(1)−B(7)	2.376(4) [2.404]
N(1)−B(9)	1.547(11)[1.565]	C(1)−C(2)	1.383(5) [1.405]
B(2)−B(3) (longest)	1.906(14) [1.902]	N(1)−B(3)	1.539(5)[1.539]
B(6)−B(11) (shortest)	1.727(14) [1.737]	B(4)−B(8) (longest)	1.903(6) [1.904]
B−B (average)	1.7845(14)	B(3)−B(6) (shortest)	1.697(5) [1.702]
P(1)−Rh(8)−P(2)	100.27(7) [98.71]	B−B (average)	1.791(5)
P(1)−Rh(8)−S(7)	96.38(7)[97.91]	S(2)−Rh(1)−P(1)	112.86(3) [104.25]
P(2)−Rh(8)−S(7)	102.05(8) [101.36]	B(3)−Rh(1)−P(1)	109.12(11) [116.25]
Rh(8)−B(9)−N(1)	120.6(5) [117.4]	C(1)−Rh(1)−P(1)	93.39(10) [93.34]
P(1)−Rh(8)−B(9)	162.4(3) [159.3]	C(2)−Rh(1)−P(1)	89.33(10) [94.11]
P(2)−Rh(8)−B(9)	95.8(3) [99.82]	C(1)−Rh(1)−C(2)	71.60(14) [71.21]
S(7)−Rh(8)−B(9)	87.1(3) [87.5]	N(1)−B(3)−Rh(1)	127.8(2) [126.9]

[a] Corresponding calculated distances for the model compounds **2a** and **3a** are enclosed in brackets.

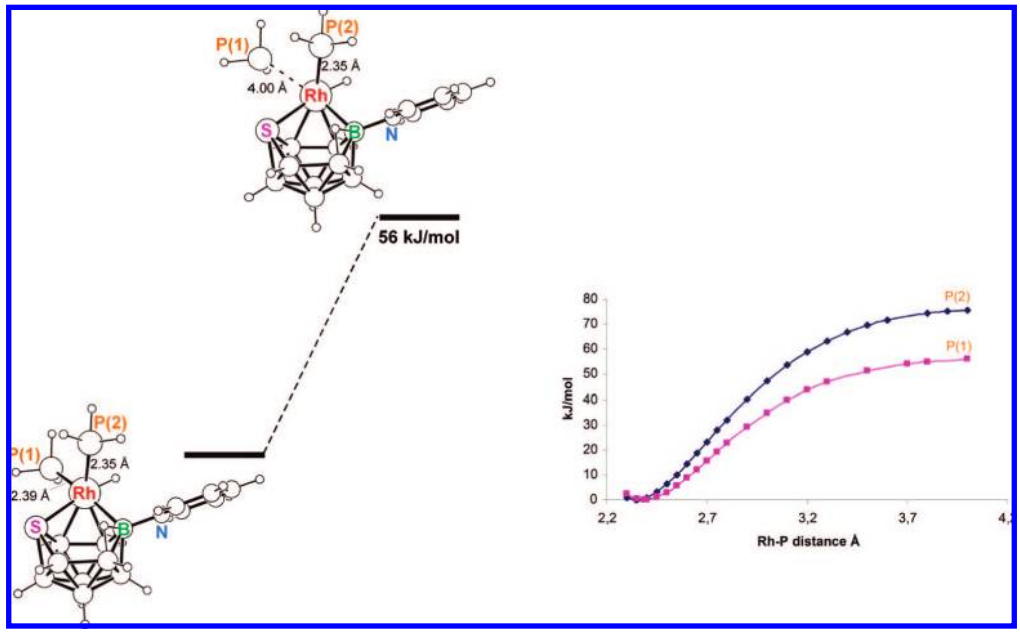

Figure 2. DFT-calculated energies (kJ/mol) computed at the B3LYP/6-31G*/LANL2DZ level for elongation of the PH_3 ligands in the model [8,8,8-$(PH_3)_2$H-9-(NC_5H_5)-*nido*-8,7-$RhSB_9H_9$] (**2a**).

As previously reported,[2] the formally unsaturated *nido*-rhodathiaborane **1** contains two main centers of reactivity: the rhodium atom and the boron atom at the 9 position. The rhodium center undergoes ligand substitution reactions and, in some cases, addition of another ligand at the third available coordination site (Scheme 1, structures **I**−**III**). It is also known that some bidentate phosphines such as dppe and dppp can attack the B(9) vertex, engendering a concomitant shift of the B−H(terminal) hydrogen atom to the metal, which leads to hydridorhodathiaborane analogues of **2** (Scheme 1, structure **I**).[2] However, these phosphine-ligated derivatives exhibit labile P−B bonds, which in dilute solutions lead to mixtures of the corresponding free phosphine and the unsaturated rhodathiaborane chelates (Scheme 1). Thus, it is somewhat surprising that the pyridine attacks selectively the boron vertex in the 9 position to afford a high yield of the new hydridorhodathiaborane **2**.

[1,1-(PPh_3)(η^2-C_2H_4)-3-(NC_5H_5)-*closo*-1,2-$RhSB_9H_8$] (3). In an atmosphere of $CH_2{=}CH_2$ the hydridorhodathiaborane **2** affords $CH_3{-}CH_3$ and [1,1-(PPh_3)(η^2-C_2H_4)-3-(NC_5H_5)-*closo*-1,2-$RhSB_9H_8$] (**3**). The solid-state structure of **3** is shown in Figure 3, where it can be seen that this rhodathiaborane is an 11-vertex cluster based on the canonical structure of an octadecahedron that may be rationalized by simple application of the Wade/Mingos approach.[35,36] The rhodium atom occupies the apical cluster position connected to six atoms in the $\{SB_9\}$ fragment with two *exo*-polyhedral metal coordination sites occupied by the PPh_3 and C_2H_4 ligands. Compound **3** is isoelectronic with previously reported 11-vertex rhodathiaboranes such as [1,1-(PPh_3)(CO)-3-(PPh_3)-*closo*-1,2-$RhSB_9H_8$],[1,1-(η^2-$Ph_2PCH_2CH_2PPh_2$)-3-(η^1-$Ph_2PCH_2CH_2PPh_2O$)-*closo*-1,2-$RhSB_9H_8$] and others,[2,3] which bear a phosphine substituent on B(3). The metrics do not differ significantly among these rhodathiaborane adducts,

Table 2. ^{11}B (96 MHz), ^{1}H (300 MHz), and ^{31}P (162 MHz) NMR Data for **1** and **2** in CD_2Cl_2 Compared to the Corresponding DFT/GIAO-Calculated ^{11}B-Nuclear Shielding Values [in brackets] for the Related P-Hydryl models **1a** and **2a**

Cluster data at 300 K

	1		**2**		
assignment[a]	$\delta(^{11}B)$	$\delta(^{1}H)$	$\delta(^{11}B)$	$\delta(^{1}H)$	$^{1}J(^{11}B-^{1}H)$
9	+12.6 [+18.7]	+3.59	+11.8 [+17.7]	NC_5H_5	
3	+16.3 [+23.1]	+4.14	+7.9 [+9.4]	+3.51	127 Hz
6	+4.5 [+7.1]	+1.56	+3.2 [+7.4]	+2.61[b]	*c*
11	+6.0 [+10.1]	+2.32	+0.3 [+2.3]	+4.12	*c*
4	+2.5 [+2.1]	+2.38	−3.7 [+0.0]	+2.84	*c*
5	−9.3 [−9.2]	+1.78	−10.0 [−10.7]	+1.84	133 Hz
10	−21.1 [−19.5]	+1.24	−18.1 [−23.0]	+0.91	*c*
1	−18.6 [−17.7]	+3.26	−25.6 [−24.9]	+1.49	142 Hz
2	−27.5 [−28.6]	+1.28	−28.5 [−28.3]	+1.12	*c*
μ (9,10)		−1.32		−1.39	

PPh_3 data for **1** at 223 K and **2** at 198 K

	1			**2**		
assignment	$\delta(^{31}P)$	$^{1}J(^{135}Rh-^{31}P)$	$^{2}J(^{31}P_1-^{31}P_2)$	$\delta(^{31}P)$	$^{1}J(^{135}Rh-^{31}P)$	$^{2}J(^{31}P_1-^{31}P_2)$
P(1) (br)	+43.0	160 Hz	36 Hz	+37.0[d]	106 Hz	16 Hz
P(2)	+20.3	128 Hz		+29.7	128 Hz	

[a] Assignments based on ^{11}B selective experiments and DFT calculations. [b] Doublet, 25 Hz. [c] Coupling constants not measured due to broadness of peaks relative to ^{1}J. [d] At higher temperatures P(1) broadens losing the $^{1}J(^{135}Rh-^{31}P)$ and $^{2}J(^{31}P_1-^{31}P_2)$ couplings; coalescence temperature 278 K.

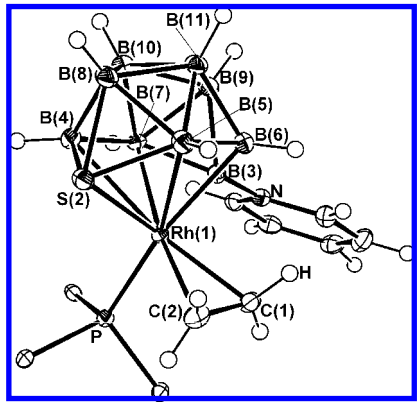

Figure 3. Molecular structure of [1,1-(PPh_3)(η^2-C_2H_4)-3-(NC_5H_5)-*closo*-1,2-$RhSB_9H_8$] (**3**).

which, as a common pattern, exhibit a Rh(1)−B(3) length shorter than the other four Rh−B distances;[2,3] this is general to 11-vertex *closo*-metallaborane and binary borane clusters due to the geometry of the canonical octadecahedron. The C═C bond distance in **3** [1.383(5) Å] is similar to those in reported ethene-ligated organometallic compounds [CSD search (version 5.29) for the M(η^2-C_2H_4) fragment; M = transition element]. The ^{1}H NMR spectrum at room temperature exhibits two multiplets at +2.27 and +2.05 ppm, which spilt into three signals of 1:1:2 relative intensity at lower temperatures and coalesce over the range 240−260 K (see Figure S5 in the Supporting Information). This temperature-dependent behavior demonstrates that the protons of the ethene ligand undergo exchange. The chemical nonrigidity of the Rh−C_2H_4 linkage has been previously reported, and the proposed mechanism consists of rotation of the ethene about the rhodium−carbon bonds.[37]

A plausible reaction pathway for formation of the ethene-ligated *closo*-rhodathiborane **3** from the *nido*-hydridorhodathiaborane **2** might start with substitution of the labile phosphine [P(1) in Figure 2] and subsequent coordination of ethene to the rhodium center. In order to identify the potential course of the reductive elimination, we carried out preliminary DFT calculations using the model [8,8-(PH_3)(η^2-C_2H_4)H-9-(NC_5H_5)-*nido*-8,7-$RhSB_9H_9$] (**3a**) as a starting point in the search for intermediates that may play a part in this reaction. The calculations suggest that reduction of the coordinated ethene group by the metal hydride produces an ethyl-ligated intermediate **Ia** stabilized by 17 kJ/mol. **Ia** can be formed as the result of an intramolecular ethene migratory insertion into the Rh−H bond followed by rearrangement of the *exo*-polyhedral ligands. Reductive elimination of the ethyl group would then be mediated by an intermediate **IIa**, which lies 8 kJ/mol higher than the ethyl-ligated intermediate **Ia**. Formation of **IIa** implies migration of the BHB hydrogen atom from the B(9)−B(10) edge to the rhodium atom and a *nido* to *closo* cluster oxidation. This transformation resembles the recently calculated transition state along the reaction coordinate for the observed fluxional process that interchanges the two enantiomeric 11-vertex *nido* cages of the parent compound **1**.[38] The final reductive elimination of ethane results in formation of a system **IIIa** that is stabilized by an agostic interaction between ethane and rhodium as illustrated in Figure 4 (Rh···H = 2.13 Å).[39] In this intermediate, ethane could be easily displaced by ethene, which is in excess in the reaction mixture.

We have not carried out a comprehensive mapping of the potential-energy surface, leading to characterization of the intermediate transition states between the potential-energy wells illustrated in Figure 4. However, these energy-optimized minima provide a useful guide for consideration of the reaction mechanism and a useful base for future experimental and calculational work. The results demonstrate that elimination of ethane from the ethene-ligated *nido*-hydridorhodathiaborane model **3a** is theoretically exothermic by 57 kJ/mol (Figure 4), which conforms to the energy required for dissociation of the PPh_3 ligand in **2** (Figure 2).

Other possible reaction pathways for formation of **3** from **2** are (i) direct loss of dihydrogen upon displacement of PPh_3 by ethene and (ii) spontaneous dehydrogenation of **2** to give a bis-PPh_3-ligated *closo* derivative that could react with C_2H_4. In this regard, we found that bubbling CO(g) through a solution of **2** in dichloromethane at room temperature affords [1,1-(PPh_3)(CO)-3-(NC_5H_5)-*closo*-1,2-$RhSB_9H_8$] (**4**) in about 20 min. In addition, the *nido*-hydridorhodathiaborane **2** loses dihydrogen after reflux in CH_2Cl_2 for 48 h, leading to formation of [1,1-(PPh_3)$_2$-3-(NC_5H_5)-*closo*-1,2-$RhSB_9H_8$] (**5**). This suggests that both pathways are in principle possible for formation of the ethene-ligated *closo*-rhodathiaborane **3**. The second route may, however, be discounted because the *nido* compound **2** is stable in CH_2Cl_2 at room temperature for at least 5 days, whereas in an atmosphere of ethene it affords the *closo* derivative **3** in 2 h (see Figures S1 and S2 in the Supporting Information). However, we cannot discount that, similarly to the CO ligand, ethene could promote dihydrogen elimination upon displacement of the labile

(37) Cramer, R.; Kline, J. B.; Roberts, J. D. *J. Am. Chem. Soc.* **1969**, *91*, 2519–2524.
(38) Macías, R.; Bould, J.; Holub, J.; Kennedy, J. D.; Štibr, B.; Thornton-Pett, M. *Dalton Trans.* **2007**, 2885–2897.
(39) Brookhart, M.; Green, M. L. H.; Parkin, G. *Proc. Natl. Acad. Sci. U.S.A.* **2007**, *104*, 6908–6914.

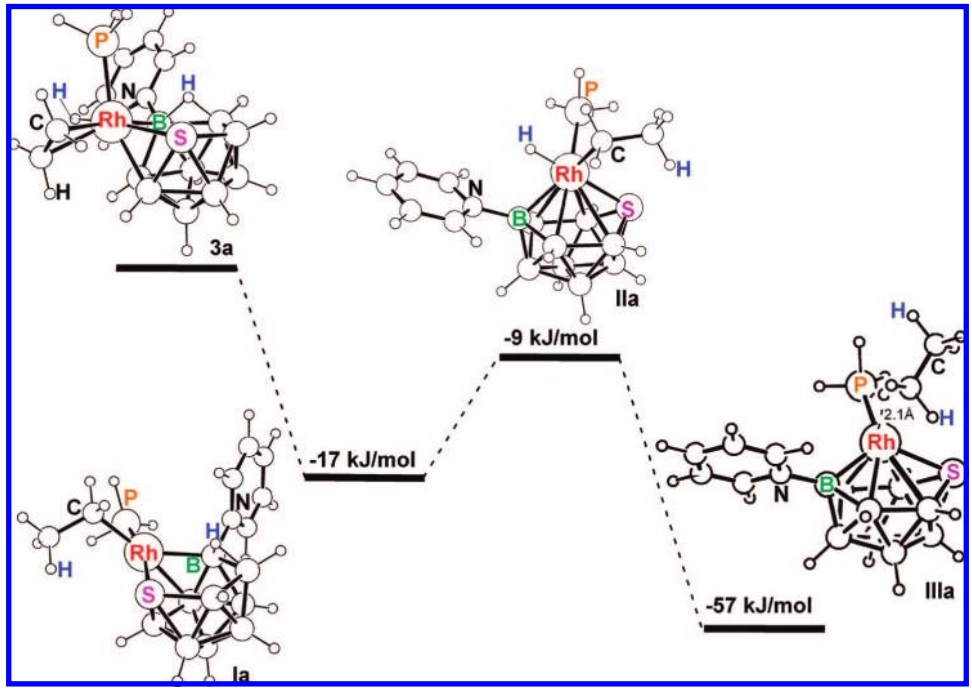

Figure 4. Potential-energy profile for the reductive elimination of $CH_2{=}CH_2$ from **3a** to give $CH_3{-}CH_3$ and a *nido* to *closo* cluster transformation.

Table 3. ^{11}B (96 MHz) and ^{1}H (300 MHz) NMR Data for **3**−**5** in CD_2Cl_2 Compared to the Corresponding DFT/GIAO-Calculated ^{11}B-Nuclear Shielding Values [in Brackets] For the Related P-Hydryl Models **3b**, **4a**, and **5a**

	3			**4**			**5**		
assignment[a]	$\delta(^{11}B)$		$\delta(^{1}H)$[b]	$\delta(^{11}B)$		$\delta(^{1}H)$	$\delta(^{11}B)$		$\delta(^{1}H)$
3	+55.7	[+58.5]	NC_5H_5	+55.4	[+58.5]	NC_5H_5	+54.6	[+58.4]	NC_5H_5
9	+26.4[c]	[+28.5]	+4.36	+28.1[e]	[+30.4]	+4.34	+27.3[g]	[+30.1]	+4.09
5	+0.8	[+9.0]	+1.80	+1.1	[+8.9]	+2.39	−0.5	[+6.7]	
4	−0.1	[+4.2]	+2.06	−0.7	[+4.2]	+1.08	(2B)	[+5.4]	+1.27
8	−14.5	[−13.3]	+2.46	−14.4	[−13.4]	+2.37	−15.2	[−12.2]	+2.16
7	−22.2	[−16.8]	+0.54	−26.1	[−21.8]	+0.66	−24.2[h]	[−18.1]	
6	−24.6	[−22.0]	−0.17	−24.4	[−17.1]	+0.08	(2B)	[−21.8]	−0.22
10	−30.3[d]	[−27.4]	+0.42	−31.9[f]	[−26.7]	+0.07	−30.4[i]	[−29.4]	
11	(2B)	[−27.0]	−0.01	(2B)	[−29.2]	+0.00	(2B)	[−29.6]	−0.27

[a] Assignments based on $^{1}H\{^{11}B\}$ selective experiments and DFT calculations. [b] Boron-bound proton resonances. [c] $^{1}J(^{11}B{-}^{1}H) = 124$ Hz. [d] Accidentally coincident ^{11}B resonances; $^{1}J(^{11}B{-}^{1}H) = 97$ Hz. [e] $^{1}J(^{11}B{-}^{1}H) = 118$ Hz. [f] Accidentally coincident ^{11}B resonances; $^{1}J(^{11}B{-}^{1}H) = 137$ Hz. [g] $^{1}J(^{11}B{-}^{1}H) = 144$ Hz. [h] $^{1}J(^{11}B{-}^{1}H) = 129$ Hz. [i] $^{1}J(^{11}B{-}^{1}H) = 139$ Hz.

PPh_3 and subsequent coordination to the rhodium atom: dihydrogen loss and ethene reductive elimination may be competing reactions in formation of **3**.

As shown in Table 3, the ^{11}B-calculated nuclear shieldings at the B3LYP/6-31G*/LANL2DZ level for the [1,1-(PH_3)(L)-3-(NC_5H_5)-*closo*-1,2-$RhSB_9H_8$] [L = C_2H_4 (**3b**), CO (**4a**), PH_3 (**5a**)] models are in good agreement with the measured ^{11}B chemical shifts for **3**−**5**. The lowest field ^{11}B resonance corresponds to the pyridine-substituted boron atom at the 3 position, which appears at around +55 ppm. The second ^{11}B resonance at low field corresponds to the boron atom in the 9 position adjacent to the B(3) atom, after which there is a significant gap (ca. 26 ppm) between these low-field resonances and the rest.

Reactions with H_2(g). The 11-vertex *closo*-rhodathiaboranes **3** and **5** react with dihydrogen (Figure 5), whereas the CO-ligated analogue **4** does not. When the metal is ethene ligated, as in compound **3**, the outcome depends on the conditions, and thus, in CH_2Cl_2 solvent with 1 equiv of free PPh_3 the reaction regenerates the *nido*-hydridorhodathiaborane **2** with formation of ethane [Figure 5a]. However, if the reaction is carried out in the absence of free PPh_3, the *closo*-rhodathiaborane decomposes within several hours. By contrast, reaction of **3** with H_2(g) in acetone leads to formation of the *nido*-hydridorhodathiaborane **2** together with decomposition of the *closo*-rhodathiaborane **3** [Figure 5c]. In the case of the bis-PPh_3-ligated *closo*-rhodathiaborane **5**, reaction with dihydrogen proceeds at the same initial rate as for **3** in the presence of PPh_3 [Figure 5b].

Hydrogenation of ethene upon reaction of [$(PPh_3)(\eta^2$-$C_2H_4)$-*closo*-$RhS_9BH_8(NC_5H_5)$] (**3**) with H_2(g) takes place most probably after formation of an ethene-ligated derivative of formulation [$(PPh_3)(\eta^2$-$C_2H_4)$H-*nido*-$RhS_9BH_9(NC_5H_5)$] for which, according to calculation, elimination of ethane should be energetically favored. Hydrogenation of ethene would lead to a coordinatively unsaturated system (**IIIa** in Figure 4) that, in dichloromethane and the absence of free PPh_3, decomposes. However, in more coordinating solvents such as acetone, the unsaturated species appears to be stabilized by formation of solvent-ligated intermediates such as, for example, [$(PPh_3)(Me_2$-$CO)RhS_9BH_8(NC_5H_5)$], which then reacts further with other molecules of **3**, sequestrating the PPh_3 ligand and leading to

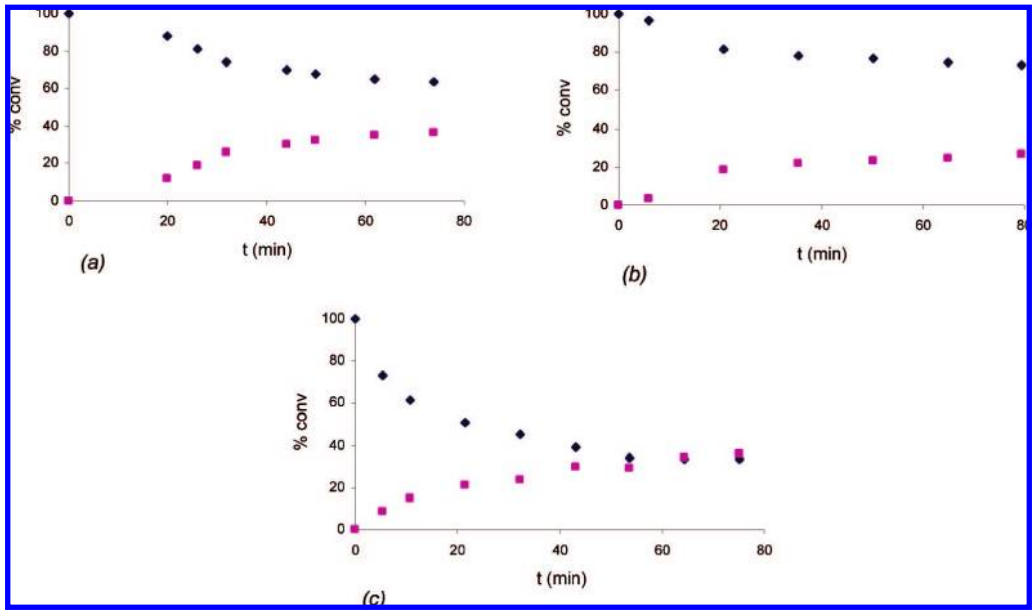

Figure 5. Plots of reaction time vs conversion based on ^{1}H NMR signal intensities for reaction of **3** and **5** with H_2(g): (a) in CD_2Cl_2 with a 1:1 ratio of **3** to free PPh_3, (b) **5** in CD_2Cl_2, and (c) **3** in $(CD_3)_2CO$ (*closo* compounds **3** and **5**, dark blue diamonds; *nido*-rhodathiaborane **2**, magenta squares).

formation of the *nido* derivative **2** and sacrificial decomposition of the parent ethene-ligated rhodathiaborane **3**.

The *closo*-rhodathiaboranes **3**−**5** may be related to the cyclopentadienyl-containing complexes $[(\eta^5\text{-}C_5H_5)Rh(\eta^2\text{-}C_2H_4)_2]$ and $[(\eta^5\text{-}C_5H_5)Rh(PPh_3)(\eta^2\text{-}C_2H_4)]$[40,41] by regarding the $\{SB_9H_8(NC_5H_5)\}$ fragment in compounds **3**−**5** as a polyhedral analogue of the C_5H_5 ligand. On the basis of this comparison, these 11-vertex *closo*-rhodathiaboranes may be thought of as 18-electron complexes of $\{Rh(PPh_3)(L)\}^+$ [L = η^2-C_2H_4 (**3**), CO (**4**), and PPh_3 (**5**)] metal moieties with the $\{SB_9H_8(NC_5H_5)\}$ fragment as a hexahapto monoanionic ligand. It has been reported that $[(\eta^5\text{-}C_5H_5)Rh(\eta^2\text{-}C_2H_4)_2]$ undergoes photochemically initiated oxidative addition of H_2(g) producing $[(\eta^5\text{-}C_5H_5)Rh(\eta^2\text{-}C_2H_4)H_2]$, which eliminates ethane in a slow thermal process.[40] Thus, the η^5-C_5H_5 organometallic analogue activates dihydrogen after formation of a coordinatively unsaturated 16-electron complex. At first sight, this single-site H_2 activation appears to be unlikely in the *closo*-rhodathiaboranes **3** and **5** since the rhodium centers are coordinatively saturated, and we have not observed *exo*-polyhedral ligand dissociation processes that could facilitate dihydrogen coordination at the metal center. On the other hand, it has been reported that heterometallic complexes of formula $[Pt_3Re_2(CO)_6(PtBu_3)_3]$ and $[Pt_2Re_2(CO)_7(PtBu_3)_3(\mu\text{-}H)_2]$ activate H_2 by addition to a single metal site without generation of a vacant site.[42] These mixed-metal clusters are highly unsaturated, and therefore, they facilitate coordination of H_2 to a metal vertex and its consequent cleavage. Compounds **3** and **5** are saturated 11-vertex *closo* clusters with 12 sep, and a priori, H_2 addition to the rhodium vertex does not appear to be favorable. However, given the stereochemical flexibility of polyhedral boron-containing compounds, a slight rearrangement of the 11-vertex *closo*-rhodathiaboranes could facilitate addition of H_2, leading to its activation (Scheme 2). In this regard, it has been reported that the *closo*-rhodadicarboranes $[3\text{-}(\eta^3\text{-}C_3H_5)\text{-}closo\text{-}3,1,2\text{-}RhC_2B_9H_{11}]$ and $[3\text{-}(\eta^3\text{-}C_8H_{13})\text{-}1\text{-}SR\text{-}2\text{-}R'\text{-}closo\text{-}3,1,2\text{-}RhC_2B_9H_9]$ (R′ = Ph, Me) activate H_2.[43,44] As a tentative mechanism, reaction with H_2 was proposed to occur through a η^3 to η^1 rearrangement of the η^3-allyl ligand followed by oxidative addition of H_2 to produce an unstable Rh(V) alkyl dihydride species or alternatively by a concerted four-center transition state involving the η^1-allyl−Rh moiety and H_2.

Single-site H_2 activation could be possible in the *closo*-rhodathiaboranes **3** and **5** through slippage of the $\{(L)_2Rh\}$ fragment above the boat-shaped {S(2)B(3)B(4)B(5)B(6)B(7)} face, leading to a vacant metal site where H_2 could bind. However, given the bifunctional character of the ethene hydrogenation mechanism illustrated in Figure 4, it is tempting to speculate that H_2 activation takes place on the rhodathiaborane cluster in a concerted manner. A possible mechanism, depicted in Scheme 2, could start with a *closo* to *isonido* rearrangement, leading to a structure that features a quadrilateral [Rh(1)B(3)B(7)-B(4)] open face.[38] This *isonido* structure would accommodate the H_2 molecule in a bridging position between the Rh(1)−B(3) edge and either of the B(3)−B(7) or B(4)−B(7) edges (*closo* numbering). Cleavage of the H−H bond would then lead directly to formation of the *nido*-hydridorhodathiaborane **2**, or it could afford an intermediate containing a Rh(1)−H−B(3) bridging hydrogen atom as in **Ib**, Scheme 2, which would then rearrange to **2**. Calculations demonstrate that an intermediate such as **Ib** lies 15 kJ/mol below the $[8,8,8\text{-}(PH_3)(L)H\text{-}9\text{-}(NC_5H_5)\text{-}nido\text{-}8,7\text{-}RhSB_9H_9]$ models [L = η^2-C_2H_4 (**3a**) and CO (**4b**)] and 9 kJ/mol above $[8,8,8\text{-}(PH_3)_2H\text{-}9\text{-}(NC_5H_5)\text{-}nido\text{-}8,7\text{-}RhSB_9H_9]$ (**2a**) (Figure 6). On the basis of these energy differences, we suggest that a Rh(8)HB(9) hydrido intermediate with the structure illustrated by **Ib** in Scheme 2 may play a role in the dehydrogenative *nido* to *closo* transformation of **2** and in the reverse H_2 activation reaction by **5**. The fact that the calculated energy

(40) Duckett, S. B.; Haddleton, D. M.; Jackson, S. A.; Perutz, R. N.; Poliakoff, M.; Upmacis, R. K. *Organometallics* **1988**, *7*, 1526–1532.
(41) Campian, M. V.; Harris, J. L.; Jasim, N.; Perutz, R. N.; Marder, T. B.; Whitwood, A. C. *Organometallics* **2006**, *25*, 5093–5104.
(42) Adams, R. D.; Captain, B. *Angew. Chem., Int. Ed.* **2008**, *47*, 252–257.
(43) Walker, J. A.; Zheng, L.; Knobler, C. B.; Soto, J.; Hawthorne, M. F. *Inorg. Chem.* **1987**, *26*, 1608–1614.
(44) Teixidor, F.; Flores, M. A.; Vinas, C.; Sillanpaa, R.; Kivekas, R. *J. Am. Chem. Soc.* **2000**, *122*, 1963–1973.

Scheme 2

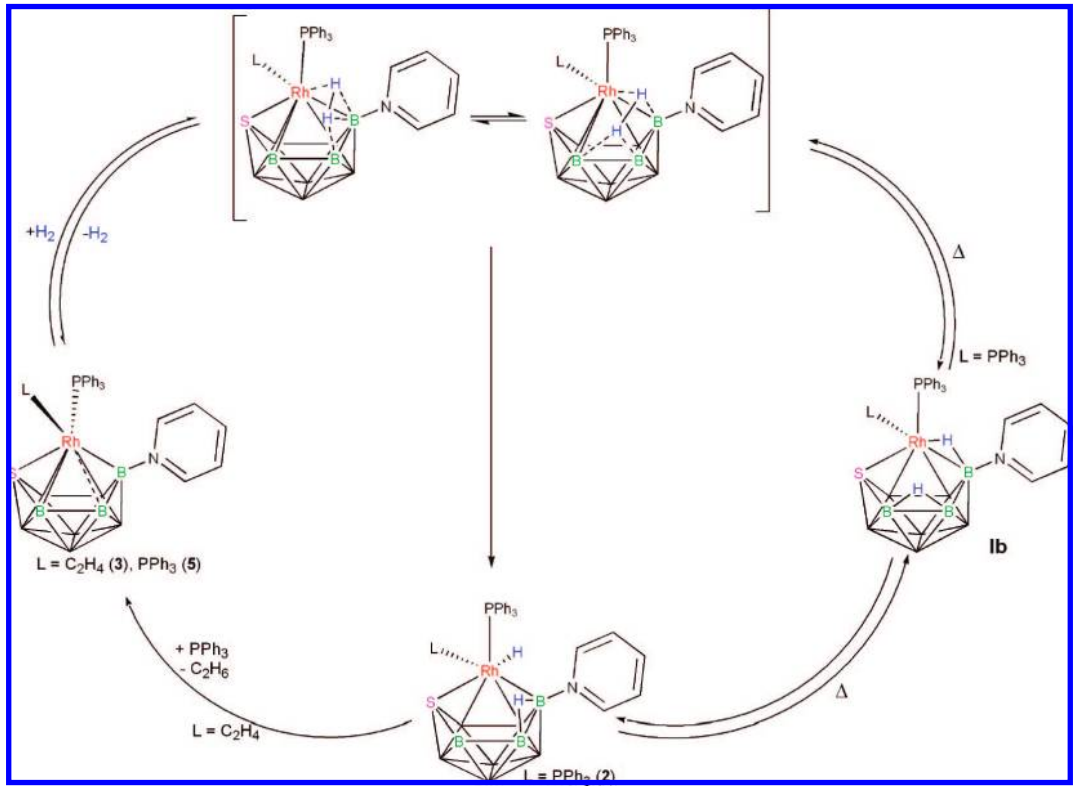

of the intermediate **Ib** is higher than that of **2a** is consistent with the stability of the *nido*-hydridorhodathiaborane **2** at room temperature and its thermally promoted *nido* to *closo* transformation. Alternatively, a CO-ligated intermediate with the structure of **Ib**, which exhibits lower energy than a putative [8,8,8-(PPh_3)(CO)H-*nido*-8,7-$RhSB_9H_9(NC_5H_5)$] (analogue of **2**), agrees with the facile H_2 elimination and *nido* to *closo* change upon reaction with CO to give **4**.

In the case of the ethene-ligated system, the PPh_3−metal-bound model with the structure of **Ib** has a calculated energy similar to the ethyl-*nido*-intermediate in the reductive elimination of ethene (**Ia** in Figure 4). In line with the proposed H_2 activation mechanism (Scheme 2), the presumed intermediate [8,8,8-(PPh_3)(η^2-C_2H_4)H-9-(NC_5H_5)-*nido*-8,7-$RhSB_9H_9$] could be another intermediate that, in the reductive elimination of ethane from the ethene-ligated *closo*-compound **3**, lies above its Rh−H−B isomer (**Ib**) and the ethyl-ligated intermediate (Figure 6).

Reduction of the 11-vertex *closo*-rhodathiaboranes **3** and **5** with H_2 is an interesting reaction since *closo* to *nido* transforma-

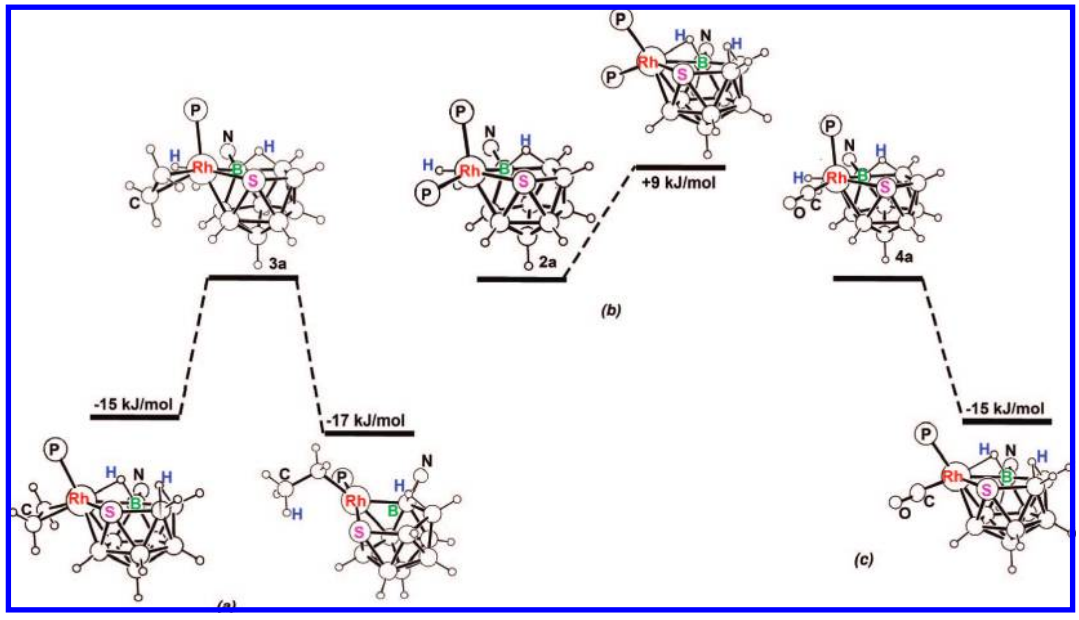

Figure 6. Energy comparisons for DFT-optimized isomeric structures of the model compounds (a) [8,8-(PH_3)(η^2-C_2H_4)-9-(NC_5H_5)-*nido*-8,7-$RhSB_9H_8$] (**3a**), (b) [8,8,8-$(PH_3)_2$H-9-(NC_5H_5)-*nido*-8,7-$RhSB_9H_8$] (**2a**), and (c) [8,8,8-(PH_3)(CO)H-9-(NC_5H_5)-*nido*-8,7-$RhSB_9H_8$] (**4b**).

Scheme 3

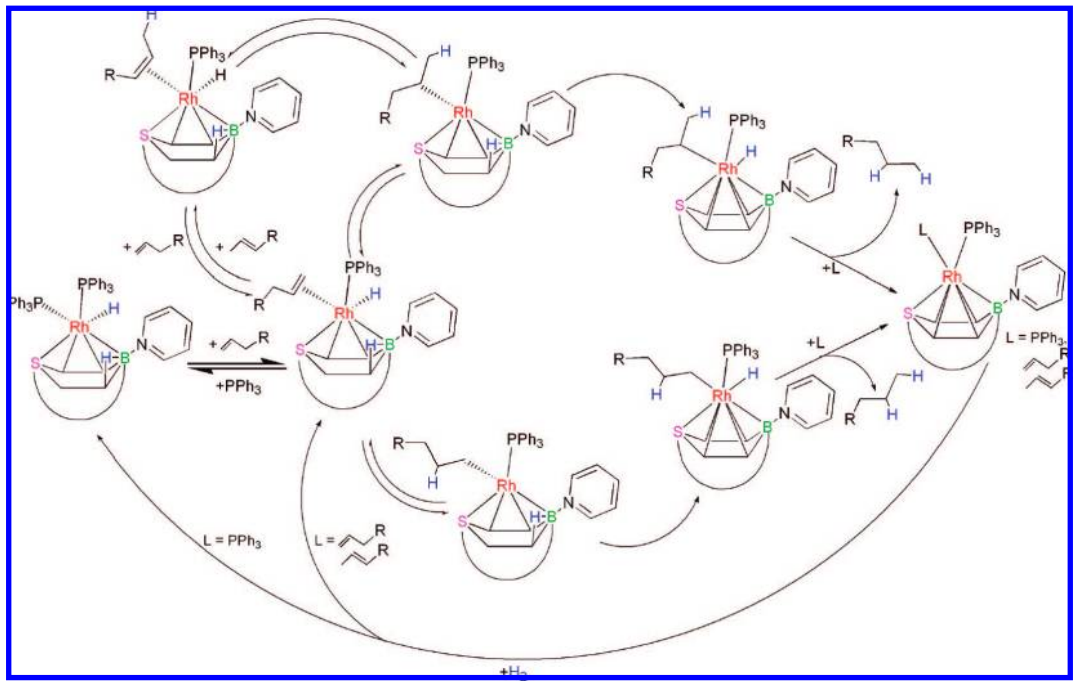

tions in polyhedral boron-containing compounds usually require strong reducing conditions.[45–49] An indication of the difficulty of this reaction is the fact that the CO-ligated *closo*-rhodathiaborane **4** does not react with H_2, and this suggests that the CO ligand stabilizes the 18-electron $\{RhPPh_3(CO)\}^+$ center by means of its higher π-back-bonding capabilities, decreasing consequently the half-cell reduction potential of the cluster. In contrast, activation of H_2 by the bis-PPh_3-ligated *closo*-rhodathiaborane **5** occurs reversibly (Scheme 2) and is thus an example of a cluster-assisted H_2 activation and dehydrogenation.

Reaction with D_2(g). To gain further insight into the mechanism of activation of H_2 by the *closo* clusters **3** and **5**, we carried out the reaction with D_2. A sample of **3** and 1 equiv of PPh_3 were placed in a screw-capped NMR tube, which was opened to an atmosphere of D_2. After 4 days, the ^{11}B and $^1H\{^{11}B\}$ NMR spectra showed a 1:1 mixture of the *nido*-hydridorhodathiaborane **2** and the bis-PPh_3-ligated *closo* compound **5**. All the BH terminal resonances corresponding to the *closo* and the *nido* species were present in the $^1H\{^{11}B\}$ NMR spectrum, but the BHB and RhH proton resonances of the *nido* compound were absent. This indicates that there is no H/D exchange at a reasonable rate between the directly boron-bound hydrogen atoms and D_2 and that the deuterium gas is activated by the *closo* clusters, leading selectively to formation of the deuterated derivative [8,8,8-$(PPh_3)_2$(D)-*nido*-8,7-$RhSB_9H_8D$-(NC_5H_5)] containing a Rh(8)−D group and a B(9)−D−B(10) bridging deuterium atom. These results are consistent with the H_2 activation mechanism proposed above.

Catalytic Hydrogenation and Isomerization of Olefins. The reaction between ethene and the *nido*-hydridorhodathiaborane **2**, combined with the activation of H_2 by **3** and **5**, opens a new door to the catalytic hydrogenation of olefins. To begin the study of the catalytic activity of the *nido*/*closo* rhodathiaborane system, we first investigated reactions of the *nido* cluster **2** with cyclohexene and 1-hexene. A 20-fold excess of cyclohexene in CH_2Cl_2 solvent at room temperature does not react with the *nido*-hydridorhodathiaborane after 3 days. However, under the same conditions 1-hexene afforded 17% of 2-hexene, 7% of 3-hexene, and 1% of hexane. This indicates that the system undergoes phosphine dissociation followed by alkene coordination and Rh−alkyl formation. Reductive elimination of the alkane is hindered by olefins higher than ethane: thus, with 1-hexene we observed formation of small amounts of hexane, but with cyclohexene no cyclohexane was formed. Steric effects may increase the energy barrier in the *nido* to *closo* transformation that, as calculated for ethene and depicted in Figure 4, may mediate on the final reductive elimination of the Rh-ligated alkyl group.

Hydrogenation experiments using **2** as the catalyst precursor and cyclohexene as substrate afforded cyclohexane. In refluxing CH_2Cl_2 the rhodathiaborane system reduces 19% of the olefin in 8 h (GC yield, unoptimized). Similarly, in catalytic amounts, the rhodathiaborane system promotes hydrogenation of 1-hexene and its isomerization to the 2- and 3-isomers. For this terminal olefin, after 5 h in CH_2Cl_2 at reflux, there is 4% formation of hexane together with 36% of the isomers 2- and 3-hexene.

On the basis of the computational and experimental studies described above we propose a mechanistic model depicted in Scheme 3 for isomerization and hydrogenation of alkenes by the **2/3/5** system. The initial step in the catalytic cycle is dissociation of the PPh_3 ligand trans to the N−B-substituted boron atom at the 9 position in **2** (Figure 2). This first step is performed by both lower and higher olefins, leading to formation of a Rh−alkyl group. At this point the system may evolve toward the final reductive elimination or β-elimination of the alkyl group. The latter reaction would be therefore responsible for the observed isomerization of terminal alkenes such as the studied 1-hexene.

(45) Evans, W. J.; Hawthorne, M. F. *Inorg. Chem.* **1974**, *13*, 869–874.
(46) Evans, W. J.; Hawthorne, M. F. *J. Chem. Soc., Chem. Commun.* **1974**, 38–9.
(47) Lopez, M. E.; Edie, M. J.; Ellis, D.; Horneber, A.; Macgregor, S. A.; Rosair, G. M.; Welch, A. J. *Chem. Commun.* **2007**, 2243–2245.
(48) Xie, Z. *Acc. Chem. Res.* **2003**, *36*, 1–9.
(49) Deng, L.; Xie, Z. *Organometallics* **2007**, *26*, 1832–1845.

According to the DFT calculations on the model **3a** final reductive elimination of the Rh−alkyl intermediate could proceed through a *closo*-hydridorhodathiaborane intermediate (Figure 4 **IIa**) formed by migration of the BHB bridging hydrogen atom to the metal center and subsequent *nido* to *closo* transformation. For alkenes higher than ethene, such as cyclohexene and 1-hexene, reductive elimination from the Rh−alkyl *nido* intermediate is hindered, suggesting that the *nido* to *closo* conversion is the rate-determining step in the hydrogenation process. After reductive elimination of the alkane, the resulting unsaturated rhodathiaborane can be stabilized by either free PPh_3 or the excess of olefin, forming the *closo* derivative **5** or alkene-ligated analogues of **3**, respectively, which, in an atmosphere of H_2, would regenerate the *nido*-hydridorhodathiaborane system, thus closing the catalytic cycle (Scheme 3).

Catalytic hydrogenation and isomerization of olefins by 12-vertex rhodacarboranes was first reported by Hawthorne and co-workers.[20–26] The catalytic activity of these compounds was attributed to formation of B−Rh(III)−H species formed by oxidative addition of terminal B−H bonds to Rh(I) centers in *exo-nido*-rhodacarboranes. These *exo-nido* precursors are best described as 16-electron Rh(I) square-planar complexes comprising an organometallic $\{RhL_2\}$ fragment bound to an 11-vertex *nido*-carborane cluster, which is acting as a bidentate chelating ligand via two B−H bonds. In the proposed mechanism[20–26] the B−H−Rh(I) species is in equilibrium with the catalytically active B−Rh(III)−H intermediates in which the *nido*-carborane is now bound in a monodentate fashion to the metal center through a boron atom. Hydrogenation of olefins by these metallacarboranes may therefore be regarded as a single-site catalytic process similar to the mechanism usually adopted by monohydride metal complexes.[50]

According to the mechanism proposed here, reduction of the alkene takes place at the rhodium center in the **2/3/5** rhodathiaborane system, but supported by calculation, the cluster then promotes the final transfer of the second hydrogen atom to the Rh−alkyl group by means of a *nido* to *closo* transformation, conferring a rhodium/thioborane bifunctional character to the process. *Nido* to *closo* transformations are fairly common in polyhedral boron chemistry.[8–14] This is, however, the first time that effective oxidation/reduction has been coupled catalytically with hydrogenation of olefins.

Conclusions

The labile nature of the PPh_3 ligand trans to the 9 boron in [8,8,8-$(PPh_3)_2$H-9-(NC_5H_5)-*nido*-$RhSB_9H_9$] (**2**) promotes isomerization and hydrogenation of olefins. DFT calculations and experimental results support a rhodium thiaborane bifunctional mechanism that, for the transfer of two hydrogen atoms to the C=C bond, combines the first part of the classical single-site monohydride route with a *nido* to *closo* cluster conversion. The resulting 11-vertex *closo*-rhodathiaboranes **3** and **5** activate dihydrogen, regenerating the *nido* parent compound **2** and initiating a new catalytic cycle. The mechanism for activation of H_2 by the *closo* species is uncertain, but according to DFT calculations and our experimental observations, a concerted process with some bifunctional character involving interaction of H_2 with the metal center and thiaborane fragment is reasonable. Dehydrogenative *nido* to *closo* oxidation of the bis-PPh_3-ligated *nido*-hydridorhodathiaborane **2** can be thermally or chemically promoted. Not surprisingly, the nature of the *exo*-polyhedral metal ligands change the reactivity of the clusters with dehydrogenation/H_2-activation being reversible for the bis-PPh_3-ligated **2/5** system and irreversible for the CO-ligated *closo* compound **4**. The reactivity of the clusters described here combines fundamental principles of organometallic chemistry and metallaborane chemistry, leading to new mechanisms for hydrogenation of olefins and activation of H_2. These results are an unusual overlap between polyhedral boron chemistry and organometallic chemistry, demonstrating that, similarly to transition-metal complexes, metallaheteroboranes may become useful reagents for functionalization of organic substrates. Although more mechanistic studies are needed in order to fully determine the kinetics of the alkene hydrogenation and activation of dihydrogen, the observed reactivity appears to be driven by the redox and structural flexibility of the 11-vertex rhodathiaboranes. These polyhedral compounds can be, in principle, tailored for chemical hydrogen storage and hydrogenation of olefins, suggesting a rich chemistry based on 11-vertex *closo*/*nido* metallaheteroboranes.

Experimental Section

General Procedures. All reactions were carried out under an argon atmosphere using standard Schlenk-line techniques.[51] Solvents were obtained from an Innovative Technology Solvent Purification System. All commercial reagents were used as received without further purification. The 10-vertex *arachno*-thiaborane salt, $CsSB_9H_{12}$, was purchased from Katchem. The starting rhodathiaborane, [8,8-$(PPh_3)_2$-8,7-$RhSB_9H_{10}$] (**1**), was prepared by published methods.[1] C, H, N, and S analyses were carried out in a Perkin-Elmer 2400 CHNS/O analyzer. Infrared spectra were recorded in KBr with a Perkin-Elmer Spectrum One spectrometer. NMR spectra were recorded on Bruker Avance 300 MHz and AV 400 MHz spectrometers using ^{11}B, $^{11}B\{^1H\}$, ^1H, $^1H\{^{11}B\}$, $^1H\{^{11}B(selective)\}$, $^{13}C\{^1H\}$, and $[^1H-^1H]$-COSY techniques. ^1H and ^{13}C NMR chemical shifts were measured relative to partially deuterated solvent peaks but are reported in ppm relative to tetramethylsilane. ^{11}B chemical shifts were measured relative to $[BF_3(OEt)_2)]$. ^{31}P (121.48 MHz) chemical shifts were measured relative to H_3PO_4 (85%). The temperature of the probe was calibrated using the temperature dependence of the chemical shifts of methanol. Mass spectrometry data were recorded on a VG Autospec double-focusing mass spectrometer, a microflex MALDI-TOF, and a ESQUIRE 3000+ API-TRAP, operating in either positive or negative modes. GC analyses were performed on an Agilent 6890N Network System equipped with a flame ionization detector and a 30 m (0.25 mm i.d., 0.25 μm film thickness) HP-Ultra-1 column. X-ray crystallographic files for **2** and **3** were deposited in the Supporting Information of the preliminary communication (ref 34).

Reaction of [8,8-$(PPh_3)_2$-*nido*-$RhSB_9H_{10}$] (1) with Pyridine. An 8 mg amount of **1** (0.0104 mmol) was dissolved in 1 mL of CD_2Cl_2 in a 5 mm NMR tube, and then 3.37 mL of pyridine was added to the bright-red solution of the rhodathiaborane. The resulting solution was examined by NMR spectroscopy at room temperature. The data revealed the quantitative formation of [8,8,8-$(PPh_3)_2$H-9-(NC_5H_5)-*nido*-$RhSB_9H_9$] (**2**). Anal. Calcd for $C_{41}H_{45}B_9NP_2RhS\cdot(CH_2Cl_2)$: C, 54.19; H, 5.09; N, 1.50; S, 3.44. Found: C, 54.24; H, 5.03; N, 1.60; S, 3.69. IR (KBr, disk): ν 2533 vs (BH), 2042 m (RhH). ^1H NMR (300 MHz, CD_2Cl_2, 300 K): δ 8.56 (m, 2H; NC_5H_5), 7.86 (m, 1H; NC_5H_5), 7.74 (t, 7.6 Hz, 1H; NC_5H_5), 7.67 (m, 1H; NC_5H_5), 7.37−7.02 (30H; $2PPh_3$), −12.46 (apparent q, $^2J(H,P) + {}^1J(H,Rh) = 18.3$ Hz, 1H, $Rh(PPh_3)_2H$). $^{31}P\{^1H\}$NMR (162 MHz, $CDCl_3$, 300 K): δ 33.2 [d, $^1J(Rh,P) = 128$ Hz; PPh_3].

(50) Oro, L. A.; Carmona, D. In *Handbook of Homogeneous Hydrogenation*; De Vries, J. G., Elsevier, C. J., Eds.; Wiley-VCH: Weinheim, Germany, 2007; Vol. 1

(51) Shriver, D. F.; Drezdzon, M. A. *The Manipulation of Air-Sensitive Compounds*, 2nd ed.; Wiley-Interscience: New York, 1986.

Table 4. Crystallographic Data and Structure Refinement Information for [8,8,8-$(PPh_3)_2$H-9-(NC_5H_5)-*nido*-8,7-$RhSB_9H_9$] (**2**) and [1-(PPh_3)-1-(η^2-C_2H_4)-3-(NC_5H_5)-*closo*-1,2-$RhSB_9H_8$] (**3**)

	2	**3**
empirical formula	$C_{41}H_{45}B_9NP_2RhS\cdot 2CHCl_3$	$C_{25}H_{32}B_9NPRh\ S\cdot CDCl_3$
mol wt	1084.71	730.12
cryst dimens (mm)	0.07× 0.10× 0.16	0.13×0.19×0.19
cryst syst	monoclinic	orthorhombic
space group	$P2_1$	*P*bca
a (Å)	12.922(3)	13.0047(8)
b (Å)	15.436(3)	19.9544(12)
c (Å)	12.930(3)	24.4736(15)
β (deg)	109.481(3)	
V (Å^3)	2431.7(8)	6350.9(7)
Z	2	8
D_{calcd} (g/cm^3)	1.480	1.527
μ (mm^{-1})	0.823	0.928
θ range (deg)	1.7−27.0	1.7−28.0
min and max trans	0.8795, 0.9469	0.8449, 0.8921
no. of reflns collected	15295	40397
no. of unique reflns (R_{int})	7878 (0.058)	7537
no. of reflns obsd ($I > 2\sigma(I)$)	6575	6324
no. of data/restraints/params	7878/25/587	7537/0/483
GOF	1.04	1.21
R indices ($I > 2\sigma(I)$)	R1 = 0.0644 wR2 = 0.1306	R1 = 0.0512 wR2 = 0.1081
R indices (all data)	R1 = 0.0814 wR2 = 0.1387	R1 = 0.0644 wR2 = 0.1306
largest diff peak and hole (e/ Å^3)	0.95, −1.73	0.95, −0.85

$^{31}P\{^1H\}$ NMR (162 MHz, $CDCl_3$, 223 K): δ 36.4 [br dd, ^1J(Rh,P) = 128 Hz, ^2J(P,P) ≈ 14 Hz not well resolved due to the broadness of the peak], 30.6 [dd, ^1J(Rh,P) = 128 Hz, ^2J(P,P) = 19 Hz]. LRMS (MALDI$^+$): *m/z* 582 [M − (PPh_3) − 2H]$^+$ (isotope envelope). Crystallographic data and structure refinement information are gathered in Table 4.

Compound **2** was also prepared on a larger scale from reaction of **1** (80 mg, 0.104 mmol) with pyridine (33 μL, 0.4173 mmol) in dichloromethane. The reaction mixture was stirred at room temperature for 2 h, and the rhodathiaborane **2** was crystallized from CH_2Cl_2/hexane to give 61 mg of product (0.07 mmol, 75 %).

Reaction of [8,8,8-$(PPh_3)_2$H-9-(NC_5H_5)-*nido*-$RhSB_9H_9$] (2) with C_2H_4. In a 5 mm NMR tube, 8 mg of **1**, dissolved in 0.7 mL of CD_2Cl_2, was treated with a four-fold excess of pyridine at room temperature to give the hydride-containing species **2**. After bubbling ethene through the solution, the reaction mixture was studied by NMR spectroscopy, which showed, after several hours, the quantitative formation of the 11-vertex *closo* rhodathiaborane, [1,1-(PPh_3)(η^2-C_2H_4)-3-(NC_5H_5)-*closo*-1,2-$RhSB_9H_8$] (**3**). The *nido* to *closo* oxidation is concomitant with reduction of ethene to yield ethane (see Figures S1 and S2 in the Supporting Information). Anal. Calcd for $C_{25}H_{32}B_9NPRhS\cdot(CH_2Cl_2)$: C, 41.59; H, 4.65; N, 1.80; S, 4.11. Found: C, 41.33; H, 4.35; N, 1.88; S, 4.48. IR (KBr, disk, 4000−450 cm^{-1}): ν 2514 vs (BH), 2468 vs (BH), 2033 w, 1619 m, 1479 s, 1458s s, 1433 s, 1263 m, 1156 m, 1090 s, 1004 m, 933 m, 744 m, 693 s, 527 s, 493 m. IR (neat, 480−200 cm^{-1}): ν 455 m (Rh−C_2H_4), ν 424 m (Rh−C_2H_4), 329 (RhP). ^1H NMR (400 MHz, CD_2Cl_2, 300 K): δ 9.28 (m, 1H, NC_5H_5), 8.57 (m, 2H, NC_5H_5), 7.74 (t, 7.6 Hz, 1H, NC_5H_5), 7.67 (m, 1H, NC_5H_5), 7.79−7.02 (15H, 1P(C_6H_5)$_3$), 2.27 (m, 2H, C_2H_4), 2.05 (m, 2H, C_2H_4). $^{31}P\{^1H\}$ NMR (121 MHz, CD_2Cl_2, 300 K): 39.7 [d, ^1J(Rh,P) = 139 Hz, 1PPh_3]. $^{13}C\{^1H\}$ NMR (75 MHz, $CDCl_3$, 300 K): δ 48.9, br s, 2C, $H_2C{=}CH_2$ (correlates with the two broad multiples at δ_H 2.27 and 2.05). $^{13}C\{^1H\}$ NMR (100 MHz, CD_2Cl_2, 193 K): δ 49.3, br d, ^{1}J(Rh,C) = 55 Hz; 46.2, br d, ^1J(Rh,C) = 40 Hz. LRMS (MALDI$^+$): *m/z* 582 [M − C_2H_4]$^+$ (isotope envelope). Crystallographic data and structure refinement information are gathered in Table 4.

Compound **3** may be prepared on a larger scale. For example, 45 mg of the ethene-ligated *closo*-rhodathiaborane was prepared by stirring of 80 mg (0.104 mmol) of **1** with four-fold excess of pyridine in 5 mL of CH_2Cl_2 for 2 h to form the hydridorhodathiaborane **2**. Exposure of the solution to an ethene atmosphere, by means of a balloon attached to the Schlenk tube, then afforded compound **3** in 4 h. Purification of the product was accomplished by crystallization from CH_2Cl_2/hexane in 70 % yield.

Reaction of 2 with 1-Hexene. In a Schlenk tube, 2 mg (0.0025 mmol) of **2** was dissolved in 0.6 mL of CH_2Cl_2 together with a 20-fold excess of 1-hexene. The resulting solution was stirred at room temperature under an argon atmosphere. The reaction was monitored by GC, and after 3 days, the mixture contained 17 % of 2-hexene, 7 % of 3-hexene, and 1 % of hexane. We did not observe formation of hexane or the associated *nido* to *closo* transformation of **2**.

Reaction of 2 with Cyclohexane. A 2 mg (0.0025 mmol) amount of **2** was dissolved in 0.6 mL of CD_2Cl_2 together with a 20-fold excess of cyclohexane. No products were observed after seven days.

[1,1-(PPh_3)(CO)-3-(NC_5H_5)-*closo*-1,2-$RhSB_9H_8$] (4). Method 1. An orange-red solution of **3** (100 mg, 0.130 mmol) in 5 mL of CH_2Cl_2 was stirred under an atmosphere of CO(g) at room temperature for 2 days during which time the initial bright-red solution became yellow. The final mixture was filtered through Celite, the solvent reduced in volume, and hexane added leading to precipitation of a yellow product, which was washed repeatedly with hexane to give 63 mg of **4** (0.104 mmol, 80 %). IR (KBr, disk, 4000−450 cm^{-1}): ν 2524 s (BH), 2474 vs (BH), 1980 vs (CO), 1619 m, 1480 m, 1456 m, 1433 m, 1167 m, 1095 m, 1005 s, 935 m, 745 m, 692 s, 526 s. ^1H NMR (400 MHz, CD_2Cl_2, 300 K): δ 9.12 (d, 6.0 Hz, 2H; NC_5H_5), 8.20 (t, 7.7 Hz, 1H; NC_5H_5), 7.64 (t, 7.7 Hz,2H; NC_5H_5), 7.40−7.26 (15H; P(C_6H_5)$_3$). $^{31}P\{^1H\}$ NMR (121 MHz, CD_2Cl_2, 300 K): 37.9 [d, ^1J(Rh,P) = 132 Hz; 1PPh_3].

Method 2. A 25 mg (0.029 mmol) amount of **2** was dissolved in 8 mL of CH_2Cl_2; then, after three freeze−pump−thaw cycles, the frozen-evacuated solution was exposed to an atmosphere of CO(g) and stirred at room temperature for 18 h. The final orange solution was reduced in volume, and hexane was added, precipitating an orange-yellow product, which was washed repeatedly with hexane to give 15 mg (0.025 mmol; 85 %) of **4**.

[1,1-$(PPh_3)_2$-3-(NC_5H_5)-*closo*-1,2-$RhSB_9H_8$] (5). A solution of **2** (30 mg, 0.035 mmol) in CH_2Cl_2 was heated at reflux in an argon atmosphere for 48 h. The final red solution was evaporated under vacuum to give a red residue, which was subsequently crystallized from dichloromethane/hexane to give 22 mg of product (0.026mmol; 74%). IR (KBr, disk, 4000−450 cm^{-1}): ν 2506 vs (BH), 1261 s (BH), 1093 s, 1022 s, 799 s, 694 m. ^1H NMR (400 MHz, CD_2Cl_2,

300 K): δ 8.90 (d, ^3J(H,H) = 5.4 Hz, 2H; C_5H_5N), 8.26 (t, ^3J(H,H) = 6.6 Hz, 1H; C_5H_5N), 7.66 (t, ^{3}J(H,H) = 6.6 Hz, 2H, C_5H_5N), 7.32−6.99 (30H, 2P(C_6H_5)$_3$). ^{31}P{^{1}H} NMR (121 MHz, CD_2Cl_2, 300 K): 39.6 [d, $^1J(^{103}Rh-^{31}P)$ = 147 Hz, 2PPh_3]. LRMS (MALDI$^+$): *m/z* 571 [M − BH − PPh_3]$^+$ (isotope envelope).

Reaction of 3−5 with H_2(g). In a typical reaction, around 10 mg (0.016 mmol) of the *closo*-rhodathiaborane was placed in a screw-capped NMR tube and dissolved in 0.6 mL of CD_2Cl_2. The NMR tube was cooled in liquid nitrogen, evacuated, and then filled with dihydrogen. The reaction was monitored at different times by ^{1}H NMR spectroscopy, and conversion was followed by integration of particular peaks in the ^{1}H{^{11}B} spectrum. The integrals for each experiment are listed in the Supporting Information. In addition, reaction of the C_2H_4-ligated *closo*-rhodathiaborane **3** with dihydrogen was studied under the following conditions: (i) In CD_2Cl_2 solvent, (iii) in CD_2Cl_2 solvent with 1 equiv of free PPh_3, and (iv) in $(CD_3)_2CO$.

Reaction of 3 with D_2(g). As in the reaction with H_2(g) above.

Catalytic Hydrogenation. To test the catalytic activity of **2** for the hydrogenation of olefins, two reactions between *nido*-hydridorhodathiaborane **2** and cyclohexene or 1-hexene were conducted in screw-capped NMR tubes: (i) 5 μL (0.050 mmol) of cyclohexane and 6 μL mL of *iso*-octane were added to **2** (2 mg, 0.003 mmol) dissolved in 0.8 mL of CH_2Cl_2; (ii) 5 μL (0.040 mmol) of 1-hexene and 6 μL of *iso*-octane were added to a solution of **2** (1.7 mg, 0.002 mmol) in 0.8 mL of $CHCl_3$. Each sample was freeze−pump−thawed and then exposed, while still immersed in the liquid nitrogen, to an atmosphere of dihydrogen (rubber-gas balloon) for 1 min. The NMR tubes were then immersed in an oil bath at 60 °C, and the reactions were monitored by GC using the *iso*-octane peak as an internal reference.

Calculations. All calculations were performed using the Gaussian 98 and Gaussian 03 packages.[52] Structures were initially optimized using standard ab initio methods with the STO-3G* basis sets for B, C, P, S, N, and H with the LANL2DZ basis set for the metal atoms. The final optimizations, including frequency analyses to confirm the true minima, together with GIAO NMR nuclear-shielding predictions, were performed using B3LYP methodology with the 6-31G* and LANL2DZ basis sets. GIAO NMR nuclear shielding predictions were performed on the final optimized geometries, and computed ^{11}B shielding values were related to chemical shifts by comparison with the calculated value for B_2H_6, which was taken to be $\delta(^{11}B)$ +16.6 ppm relative to the $F_3B\cdot OEt_2$ = 0.0 ppm standard. In each case the compounds were modeled using hydrogen atoms rather than phenyl groups on the phosphine ligands in order to reduce computation time.

Acknowledgment. This work was supported by the Ministerio de Educación y Ciencia (MEC, Spain) (Factoría de Cristalización, CONSOLIDER INGENIO-2010 and grant CTQ2006-01629). R.M. thanks the MEC-Universidad de Zaragoza and the European Social Fund for his Research Contract in the framework of the "Ramón y Cajal" Program. A.A. thanks the IUCH for a fellowship. J.B. thanks professors J.D. Kennedy and M.J. Pilling for the use of facilities. J.B. was supported in part by the Czech Academy of Sciences Grant No. IAA400320601 and the Grant Agency of the Czech Republic Project No. 203 3982.

Supporting Information Available: Complete ref 52; figures for ^{1}H and ^{31}P spectra of **2** and **3**; attached proton test spectrum of **2**; conversions of **2**, **3**, and **5** in their reaction with H_2; GC data; computational details, coordinates of optimized geometries, and calculated energies for all themodel compounds. This material is available free of charge via the Internet at http://pubs.acs.org.

JA802993M

(52) Pople, J. A., et al. *Gaussian 03*, revision B.05; Gaussian Inc.: Wallingford, CT, 2004.